Liquid crystallography: 3D microdroplet arrangements using microfluidics†

Lingling Shui,*[a] E. Stefan Kooij,[b] Daniël Wijnperlé,[a] Albert van den Berg[a] and Jan C. T. Eijkel[a]

Received 28th April 2009, Accepted 22nd May 2009
First published as an Advance Article on the web 9th June 2009
DOI: 10.1039/b908498c

Monodisperse liquid particles (femtolitre oil droplets) are shown to self-organize into three-dimensional (3D) close-packed face-centered cubic (fcc) arrangements. Droplets were formed at a nanochannel–microchannel interface, and the formation of these arrangements occurred at certain flow-rate ratios of oil and water. The remarkably robust and stable structures formed in two different 'crystallographic' orientations of a face-centered cubic lattice, fcc(100) and fcc(111), as evidenced by the occurrence of square and hexagonal patterns at the plane adjacent to the channel wall. The orientation was found to depend on the oil-to-water flow-rate ratio. Similar to solid state crystals, 'crystallographic' features were observed, such as dislocation lines and defects. The 3D arrays presented in this work could provide platforms for a number of applications.

1. Introduction

Pattern formation in general is ubiquitous in nature,[1–3] and fluid systems in particular provide a fertile ground for studies of the self-organization of complex superstructures.[4,5] Periodic organization of chemical, mechanical, optical, electrical or magnetic properties is important in materials. Regular three-dimensional (3D) arrays of solid particles have shown many possible applications, for example as photonic crystal structures, liquid chromatography packing materials and data storage.[6–10] The use of liquid particles instead of solid particles leads to a simple way of tuning the array properties due to the large variation in chemical and optical properties of liquids.

Liquid flows confined within microfluidic devices offer specific and unique fluid dynamics and boundary conditions, which may be used to induce pattern formation of many sorts. Recently, the creation and flow of nano- and micro-particles (colloid particles, liquid droplets or gas bubbles) in microfluidic systems has attracted considerable attention.[11–15] The micrometre length scale is sufficiently small to warrant neglecting inertial and gravity effects in the fluid (low Reynolds and Bond numbers).[16,17] These dynamical systems can therefore be generally described by simple physical models involving a limited number of variables.

Several groups have investigated the formation of periodic two-dimensional (2D) arrangements of fluid (liquid or gas) particles inside microchannels.[18–21] Generally, highly complex structures result from the drive for the system to minimize the local interfacial energies. In this respect, fluid particles, which are 'soft' and deformable, are distinctly different from solid particles. The self-organization of the fluid particles is seen to be determined by the particle size, the channel geometry, the volume fractions and the relative fluid pressures. In most previous reports on droplet formation and organization in microchannels, particles were created by shearing the dispersed liquid (oil or water) into the continuous phase (water or oil). Typically, the volume of the generated droplets (or bubbles) for these systems is comparable to, or larger than, the volume of the largest sphere that can be inscribed inside the microchannel. In these cases only 2D structures will be formed.

In contrast to these previous results, we report on the creation of droplets with a diameter considerably smaller than the microchannel height, therewith allowing for multiple layers of droplets to be assembled inside the microchannel. For their formation we use a device with a junction between a nanochannel and microchannel, where droplets are formed by capillary instability.

2. Experimental

2.1 Device design

The channel structure used for the experiments is shown in Fig. 1 (top). Water and oil are introduced into separate inlets, both into

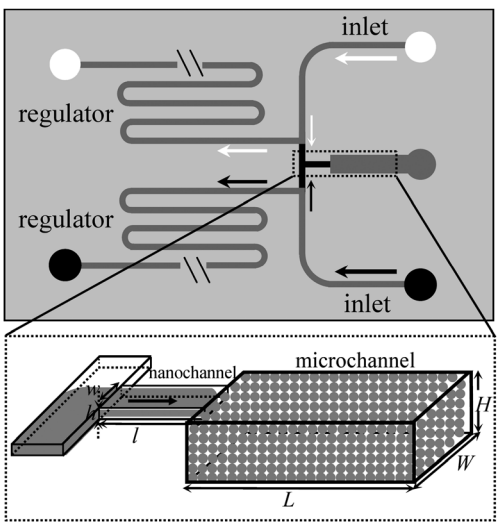

Fig. 1 Schematic representation of the glass channel structure used. Water enters from the top inlet and oil from the bottom inlet. The flow is split in a ratio of 1 : 10 000 between the microchannel regulator and the nanochannel section. h, w and l are nanochannel height, width and length, respectively; and H, W, L are microchannel height, width and length, respectively.

[a]*BIOS/Lab-on-a-Chip Group, MESA+ Institute for Nanotechnology, University of Twente, The Netherlands. E-mail: l.shui@utwente.nl; Fax: +31-(0)53-489-3595; Tel: +31-(0)53-489-2722*
[b]*Solid State Physics, MESA+ Institute for Nanotechnology, University of Twente, The Netherlands*

† Electronic supplementary information (ESI) available: Movies of the square arrangement (fcc(100) facet) and the hexagonal arrangement (fcc(111) facet) of microdroplets at the plane adjacent to the channel wall. See DOI: 10.1039/b908498c

microchannel sections (gray). These microchannel sections connect to a T-shaped nanochannel section (black). The volume flow rates of oil and water in the nanochannel section are determined by the oil and water inlet pressures and the relative hydrodynamic flow resistances of the microchannel and nanochannel sections. For both oil and water, the volume flow was split in a ratio of 1 : 10 000 between the nanochannel section and the microchannel section. This allowed the use of normal syringe pumps to produce very low nanochannel flow rates. The nanochannel section consisted of two identical inlets, and a constriction channel which was connected to a microchannel, see Fig. 1 (bottom). Droplets formed at the interface between the nanochannel and the microchannel due to the native hydrophilicity of the glass and the oil-in-water emulsion. The nanochannel inlet channel and constriction channel dimensions are: height (h) = 500 nm, width (w) = 10 μm and length (l) = 500 μm; and the microchannel dimensions are: height (H) = 10 μm, width (W) = 50 or 100 μm, length (L) = 5 mm.

2.2 Fabrication and setup

The devices were fabricated in glass using standard microlithographic techniques. Nanochannels and microchannels were etched into a borosilicate glass wafer using buffered hydrofluoric acid and 25% hydrofluoric acid solutions, respectively. Connection holes were drilled in a second borosilicate glass wafer using powder blasting techniques. Subsequently, these two wafers were aligned and thermally bonded together. We diced the bonded wafers to 10 mm × 20 mm sized chips, which were mounted in a home-made chip holder and connected to gas-tight syringes (Microliter Syringes, Hamilton) *via* nanoport connectors (Upchurch Scientific). Harvard syringe pumps (PHD 22/2000, Harvard Apparatus) were used to drive the liquid flow. Due to the flow split ratio of 1 : 10 000, flow rates down to 10^{-5} μL min^{-1} could be obtained in the nanochannel section. The two-phase flow was visualized by an inverted microscope (Leica DMIRM) and recorded using a CCD camera (Orca ER).

2.3 Fluids

The water phase was made fluorescent (appearing white in the microphotographs) by dissolving fluorescein sodium salt (Sigma-Aldrich Chemie GmbH, Germany) in deionized water at a final concentration of 0.01 mol L^{-1} (η_w = 1 mPa s). The organic phase (dark in the images) consisted of hexadecane (Sigma-Aldrich Chemie GmbH, Germany) without any added fluorescent markers (η_o = 3 mPa s). Surfactants were used to stabilize generated droplets. The surfactants used were sodium dodecyl sulfate ($CH_3(CH_2)_{11}OSO_3Na$, SDS 99+%,), Tween 80, and Span 80 (all Sigma-Aldrich Chemie GmbH, Germany). Solutions were prepared by dissolving hydrophilic surfactants (SDS and Tween 80) in water or hydrophobic surfactant (Span 80) in hexadecane. The surfactant concentrations were, in all cases, above the critical micelle concentration. Solutions were degassed under vacuum for 1 h.

3. Results and discussion

3.1 3D Microdroplet arrays

When the co-flowing oil and water exit from the nanochannel into the microchannel (see Fig. 1), oil droplets are formed in the water phase at the junction of the nanochannel and microchannel. Over a wide range of flow conditions (oil and water flow rates of 10^{-5}–10^{-3} μL min^{-1}), the diameter of the observed oil droplets is independent of flow rate and remarkably monodisperse. This can be explained as follows. At the low flow rates used, shearing and squeezing can be excluded as droplet formation mechanisms, and instead the capillary pressure difference between the nanochannel and microchannel will dominate droplet formation, which occurs as a result of capillary instability.[22] Since this pressure difference is constant, the diameter of the obtained droplets is independent of flow rate and the droplets are monodisperse. By varying the nanochannel height and therefore the capillary pressure difference, we could obtain monodisperse droplets with sizes in the range of 0.5–10 μm. For the experiments reported in this paper, we used a device with h = 500 nm, w = 10 μm, l = 500 μm, H = 10 μm, W = 50 or 100 μm and L = 5 mm, resulting in droplets that were 2.5 ± 0.1 μm in diameter (standard deviation estimated from the measurement error). The emulsion that was formed remained stable for at least several weeks.

Optical microscopy on the microchannel region reveals that, depending on the flow conditions, the oil droplets self-organize into highly ordered 3D structures in the microchannel. Depending on the relative flow rates of water and oil, different droplet patterns at the plane adjacent to the channel wall are therefore observed, as displayed in Figs. 2(a–d). Four different patterns were observed at this plane: disordered, square (fcc(100)), hexagonal (fcc(111)) and coalescent. The corresponding FFT (Fast Fourier Transform) images are also shown. The FFT images clearly show the highly ordered, nearly perfect square (Fig. 2b) and hexagonal (Fig. 2c) arrangements of the liquid droplets at the plane, as witnessed by the periodic structures (see ESI†). The absence of bright spots in the other two FFT images (Figs 2a and 2d) represents the absence of long-range directional order, in agreement with the random distribution of droplets in the disordered and coalescent arrangements. Careful inspection of the FFT image for the disordered arrangement reveals a ring-like structure. Two concentric rings, with a ratio of 1.7 for their radii, reveal the short-range ordering within the disordered droplet phase. A polycrystalline phase would also yield rings in the FFT image, but from Fig. 2a it is obvious that this is not the case. The short-range ordering, *i.e.* a minimum distance between nearest-neighbour droplets, arises from the fact that all droplets have the same size and that there is a net short-range steric repulsion. For the coalescent arrangement, the high degree of polydispersity leads to the absence of such a concentric ring pattern.

The flow conditions were seen to affect the process of droplet formation and the self-organization into ordered superstructures. In Fig. 2e the occurrence of the various different patterns at the plane adjacent to the channel wall are shown as a function of the oil and water volume flow rates (Q_o and Q_w, respectively). In this flow map, four well-separated regimes are found: (i) At low oil-to-water flow-rate ratios ($Q_o < 2Q_w$) the oil droplet flow is disordered in the microchannel after generation. (ii) When the flow-rate ratio rises above a certain threshold ($Q_o > 2Q_w$), the oil droplets self-organize into ordered square patterns at the wall. (iii) At still higher flow rate ratios ($Q_o > 7Q_w$) a hexagonal pattern is observed at the channel wall. (iv) Above a certain oil flow rate ($Q_o > 3 \times 10^{-4}$ μL min^{-1}) the oil droplets start to coalesce in the microchannel. These observed arrangements remain intact when the droplets continuously flow downstream and slightly reorganize with time (interchanging droplets and rotation of domains).

As mentioned in the experimental section, different surfactants were used to create stable droplets. Very similar flow phases are

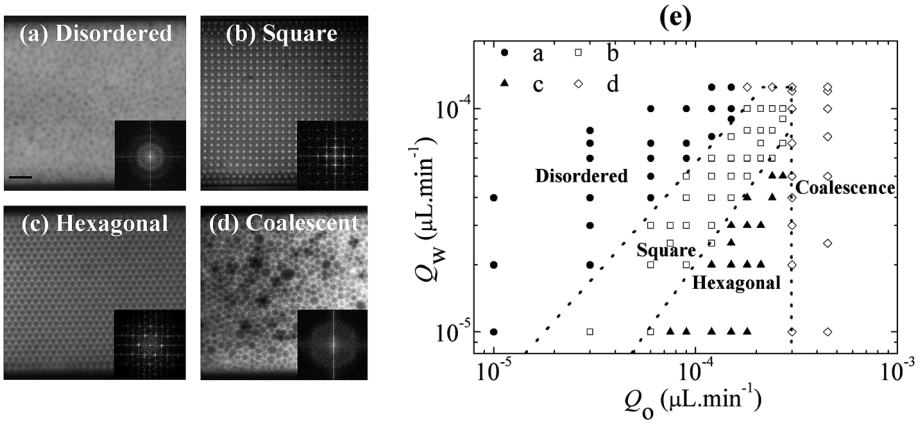

Fig. 2 (a–d) Snapshots of the oil droplet patterns observed at the plane adjacent to the microchannel wall. The insets represent their corresponding FFT images, which reveal random patterns for (a) disordered and (d) coalescent structures, and nearly perfect (b) square and (c) hexagonal patterns in microchannels. (e) Structural domains vary with the volume flow rates of oil (Q_o) and water (Q_w). The pattern is considered to be square if > 50% of the area is occupied by square lattice. The same criterion was applied to the hexagonal case. The surfactant used in these experiments was Tween 80 at 1 wt% concentration. The scale bar is 10 μm.

obtained using various surfactants: 1 wt% Span 80, 0.3 wt% SDS and 1 wt% Tween 80. Apparently, the precise nature of the surfactant does not play a significant role in defining microdroplet size and self-organization.

3.2 Liquid crystallography

The square and hexagonal arrangements unambiguously demonstrate well-defined 3D lattices of microdroplets. Fig. 3a shows typical microscopic images of hexagonal and square arrangements of the droplets observed at the plane adjacent to the channel wall. Since the oil droplet diameter is 2.5 μm and the channel height amounts to 10 μm, there are a number of droplet layers in the microchannel, as could be visualized by moving the focal point of the microscope deeper into the channel (Fig. 3b, the black dashed and white solid lines indicate patterns in two different layers). If we hypothesize that both observed patterns correspond to the same specific 3D organization, but viewed in different orientations, the observed distances between the droplets in the square and hexagonal arrangements should be related. This was indeed confirmed, and we conclude that the droplets with diameter d (due to their close packing, d is equal to the minimum center-to-center distance between droplets) are organized in a face-centered cubic (fcc) structure (see Fig. 3c). The size of the corresponding unit cell (indicated by the white cube in Fig. 3c) with lattice parameter a amounts to $a = d\sqrt{2} = 3.5$ μm, since the center-to-center distance between the droplets in the hexagonal pattern corresponds to the half of the diagonal of a face of this unit cell. The highly ordered patterns we observe in Figs 3a and 3b are thus related to two different 'crystallographic' orientations of the fcc arrangement in both droplet arrays. The square pattern corresponds to the (100) plane, while the hexagonal arrangement corresponds to the (111) plane. The organized structures proved to be very stable (typically for several weeks) and highly reproducible under the same flow conditions. This suggests that the patterning can be solidified to form 3D structures which will be very useful for real-life applications.[8–10,23,24]

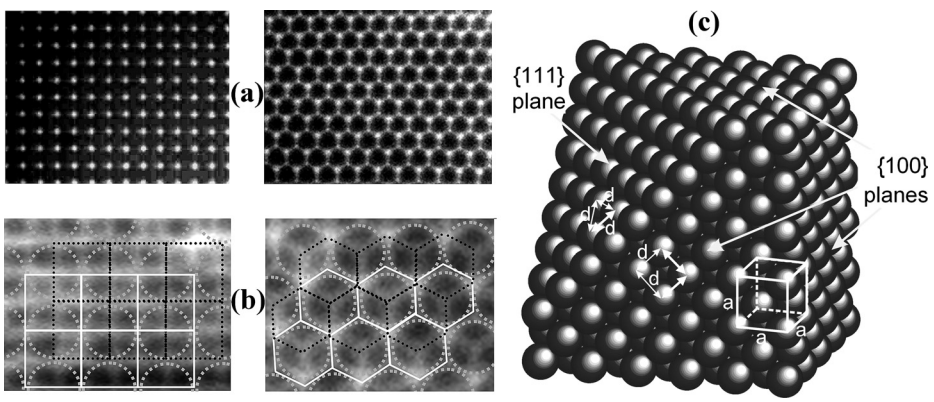

Fig. 3 (a) Self-organized square (left) and hexagonal (right) arrangements observed at the plane adjacent to the channel wall. (b) Microphotographs demonstrate two layers of the arrangements where the gray dotted circles indicate oil droplets and the black dashed lines and white solid lines are drawn to indicate the arrangements in the two different layers. Both arrangements were calculated to represent the same crystal structure in different rotations. (c) Schematic representation of the face-centered cubic (fcc) crystal structure, where the square and hexagonal patterns correspond to fcc (100) and (111) planes, respectively. The white cube frame indicates a unit cell, with lattice parameter a, while the smallest center-to-center particle distance d is indicated in the different planes.

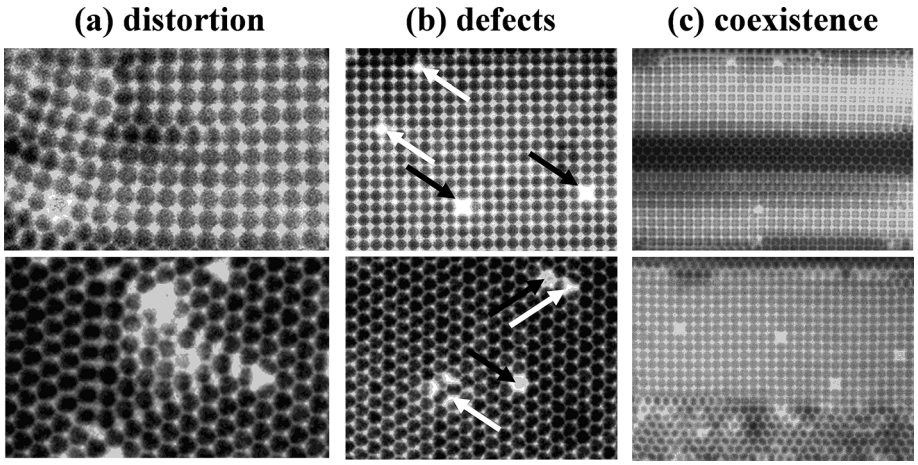

Fig. 4 Different dynamic organizations of liquid particles. (a) Distortion in square (top) and hexagonal (bottom) patterns. (b) Defects in square (top) and hexagonal (bottom) patterns. The black arrows indicate defects in the top layer, or a deeper layer where the particles have the identical position. The white arrows indicate vacancies that are in the layer beneath the top layer. (c) Coexistence of square and hexagonal patterns in the microchannel.

Since the structures form in a dynamical situation, perturbations that occur will induce instability. Therefore, the system does not always display perfect packing of the droplets in the microfluidic device. We observed 'grain' boundaries, 'dislocations' and vacancy defects in the patterns, as well as the coexistence of square and hexagonal patterns (Fig. 4). Owing to the fluorescence of the water phase, vacancies in the oil droplet 'crystals' are exposed as the bright spots in the patterns (both in square and hexagonal arrangements).

3.3 Phase transition

Now we turn to the two different orientations of the fcc superstructure, *i.e.* regimes (ii) and (iii) described above, as witnessed by the square and hexagonal arrangement of microdroplets at the plane adjacent to the channel wall. We believe that the oil volume fraction $V_f = Q_o/(Q_w + Q_o)$ mainly determines the observed arrangements. The square arrangement occurs at $V_f > 0.67$. In this arrangement the vertical space needed in the microchannel for n layers is $d(1 + (n - 1)/\sqrt{2})$. Five droplet layers then correspond to a height of 9.57 μm and will thus fit into the channel. Assuming five layers, the packing density is 0.65, agreeing well with the observed transition from disordered to square at $V_f = 0.67$. The transition from square to hexagonal is seen to occur approximately at $V_f > 0.87$. This is higher than the packing density for the fcc structure (0.74), so that the rotation of the fcc structure must be accompanied by a deformation of the oil droplets. In this arrangement the vertical space needed in the channel for n layers is $d(1 + (n - 1)/\sqrt{(3/2)})$. Thus, if five layers occur in the hexagonal fcc(111) arrangement, the packing density is 0.75 and the structure height is 10.66 μm so that deformation will occur in the 10 μm channel. Such droplet deformation was indeed observed in the hexagonal fcc(111) pattern.

A sufficiently large perturbation was seen to lead to a transition of the system from one organization pattern to another, *i.e.* to a re-orientation of the 3D superstructure. As already shown in Fig. 2e, a hexagonal-to-square transition is observed when decreasing the oil-to-water volume flow-ratio to below 2. Inversely, upon increasing the relative oil flow rate to a value above 2, a transition from square to hexagonal arrangement is induced.

The re-orientation mechanism described in the previous paragraph pertains to quasi-static conditions, *i.e.* in which the fluid flow is constant. Now we consider the situation in which the flow of both water and oil is abruptly interrupted; the new situation is referred to as the flow-free state. Starting from a quasi-static state with hexagonally arranged droplets at the plane, initially we observe a gradual transition from the hexagonal to the square 'phase', typically within a few hours (Figs. 5(a–c)). Assuming that the hexagonal fcc

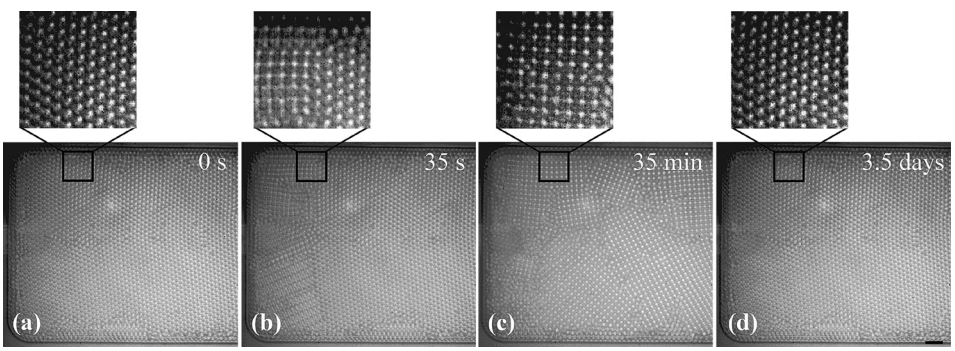

Fig. 5 Transition of hexagonal–square–hexagonal at the flow-free state: (a) hexagonal, (b) hexagonal + square, (c) square, and (d) hexagonal. The scar bar is 10 μm.

orientation is accompanied by a slight droplet deformation, we hypothesize that the system in this phase relaxes to the lower energy state in which droplets are non-deformed. For this to happen, the oil volume fraction inside the microchannel must decrease, and the source of water for this process could be the microchannel water outlet reservoir and the emulsion outlet reservoir. Simultaneously, a slight retraction of the oil thread into the nanochannel is indeed observed, which can also only occur as the result of an influx of water. After prolonged relaxation of the flow-free state, typically for a few days, we often observe a transition from the square to hexagonal arrangement (Figs. 5c and 5d). In this case, we can account for the observations by considering the gradual disappearance of water from the system by evaporation from the outlet reservoir. Therefore, at the free-flow state, we can obtain a hexagonal–square–hexagonal transition starting from a hexagonal arrangement or a square–hexagonal transition starting from a square arrangement.

4. Conclusions

We have demonstrated a new nano–micro fluidic system which enables multilayer emulsion formation and patterning. Oil droplets, created at the junction of a nanochannel and a microchannel, are highly monodisperse with a size independent of the flow rate and the emulsion is remarkably stable over a wide range of flow conditions. Over a large range of absolute and relative flow rates, the oil droplets furthermore self-organize into a close-packed 3D superstructure, which can be identified as a face-centered cubic arrangement. Different orientations of this face-centered cubic lattice, depending on the specific flow conditions, are observed by square or hexagonal droplet arrangements in the plane adjacent to the channel wall, corresponding to (100) and (111) facets. In these dynamical multiphase fluidic systems, perturbations, mainly from the flow of the liquids, induce dislocation lines and defects, and also transitions between square and hexagonal patterns. This study is expected to lead to a better understanding of 3D periodic close-packed two-phase metastable systems and their applications in real life. The incorporation of large quantities of monodisperse domains, in an organized fashion, within suitable matrices is useful. The liquid particle patterning offers a flexible alternative to solid particle arrays for use in *e.g.*, photonic crystal structures (opals and inverted opals), liquid chromatography packing materials and data storage.[9,10,23–27] The effects of channel geometry, droplet size and chemical issues will be further studied in the future.

Acknowledgements

This research was supported by the Dutch Ministry of Economic Affairs through a Nanoimpuls grant.

References

1 E. Cox, *Nature*, 1998, **396**, 731.
2 S. H. Lim, S. Che, H. Yoshitake and T. Tatsumi, *Chem. Lett.*, 2005, **34**, 792.
3 L. J. Fu, T. Zhang, Q. Cao, H. P. Zhang and Y. P. Wu, *Electrochem. Commun.*, 2007, **9**, 2140.
4 J. P. Gollub and J. S. Langer, *Rev. Mod. Phys.*, 1999, **71**, S396.
5 M. C. Cross and P. C. Hohenberg, *Rev. Mod. Phys.*, 1993, **65**, 851.
6 Y. A. Vlasov, X. Z. Bo, J. C. Sturm and D. J. Norris, *Nature*, 2001, **414**, 289–293.
7 S. K. Lee, G. R. Yi and S. M. Yang, *Lab Chip*, 2006, **6**, 1171.
8 S. A. Vanapalli, C. R. Iacovella, K. E. Sung, D. Mukhija, J. M. Millunchick, M. A. Burns, S. C. Glotzer and M. J. Solomon, *Langmuir*, 2008, **24**, 3661–3670.
9 C. W. Kuo, J. Y. Shiu, K. H. Wei and P. Chen, *J. Chromatogr.*, 2007, **1162**, 175.
10 A. Ethirajan, U. Wiedwald, H. G. Boyen, B. Kern, L. Y. Han, A. Klimmer, F. Weigl, G. Kastle, P. Ziemann, K. Fauth, J. Cai, R. J. Behm, A. Romanyuk, P. Oelhafen, P. Walther, J. Biskupek and U. Kaiser, *Adv. Mater.*, 2007, **19**, 406.
11 N. V. Dziomkina and G. J. Vancso, *Soft Matter*, 2005, **1**, 265–279.
12 M. Joanicot and A. Ajdari, *Science*, 2005, **309**, 887–888.
13 T. Thorsen, S. J. Maerkl and S. R. Quake, *Science*, 2002, **298**, 580–584.
14 B. H. Weigl and P. Yager, *Science*, 1999, **283**, 346–347.
15 N. J. Carroll, S. B. Rathod, E. Derbins, S. Mendez, D. A. Weitz and D. N. Petsev, *Langmuir*, 2008, **24**, 658–661.
16 T. M. Squires and S. R. Quake, *Rev. Mod. Phys.*, 2005, **77**, 977.
17 L. Shui, J. C. T. Eijkel and A. van den Berg, *Sens. Actuators, B*, 2007, **121**, 263.
18 T. Thorsen, R. W. Roberts, F. H. Arnold and S. R. Quake, *Phys. Rev. Lett.*, 2001, **86**, 4163.
19 J. P. Raven and P. Marmottant, *Phys. Rev. Lett.*, 2006, **97**, 154501.
20 P. Garstecki and G. M. Whitesides, *Phys. Rev. Lett.*, 2006, **97**, 024503.
21 A. Woodward, T. Cosgrove, J. Espidel, P. Jenkins and N. Shaw, *Soft Matter*, 2007, **3**, 627–633.
22 L. Shui, F. Mugele, A. van den Berg and J. C. T. Eijkel, *Appl. Phys. Lett.*, 2008, **93**, 153113.
23 G. M. Gratson, F. Garcia-Santamaria, V. Lousse, M. J. Xu, S. H. Fan, J. A. Lewis and P. V. Braun, *Adv. Mater.*, 2006, **18**, 461.
24 A. Penrose, P. Myers, K. Bartle and S. McCrossen, *Analyst*, 2004, **129**, 704–709.
25 G. R. Yi, S. J. Jeon, T. Thorsen, V. N. Manoharan, S. R. Quake, D. J. Pine and S. M. Yang, *Synth. Met.*, 2003, **139**, 803.
26 V. N. Manoharan, A. Imhof, J. D. Thorne and D. J. Pine, *Adv. Mater.*, 2001, **13**, 447.
27 J. Wijnhoven and W. L. Vos, *Science*, 1998, **281**, 802–804.

